

Controlling the Minimal Self Assembly of “Complex” Polyoxometalate Clusters

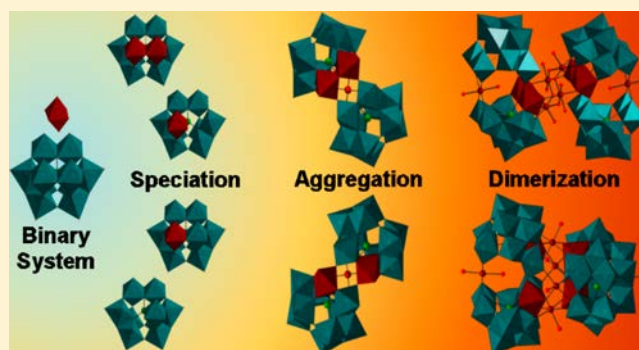
Ross S. Winter, Jamie M. Cameron, and Leroy Cronin*

School of Chemistry, WestCHEM, University of Glasgow, Glasgow, G12 8QQ, U.K.

S Supporting Information

ABSTRACT: Despite the vast number of polyoxometalate clusters now known, an ongoing and important challenge is to understand causality in the assembly of “complex” clusters at a mechanistic level, since this is the only way the rational, targeted synthesis of new compounds will ever be achieved. Often, the complexity of the reactions themselves makes such investigations near impossible, as very small changes can often make dramatic differences. Herein, we explore a very simple [A + B] binary synthetic system that gives rise to the facile assembly of two isomeric anions, $[\text{Fe}^{\text{III}}(\text{H}_2\text{O})_2\{\gamma\text{-Fe}^{\text{III}}\text{SiW}_9\text{O}_{34}(\text{H}_2\text{O})\}_2]^{11-}$ (1) and $[\text{Fe}^{\text{III}}(\text{H}_2\text{O})_2\{\gamma\text{-Fe}^{\text{III}}\text{SiW}_8\text{O}_{33}(\text{H}_2\text{O})_2\}\{\gamma\text{-SiW}_{10}\text{O}_{35}\}]^{11-}$ (2), which can be formed as individual and dimeric species (3) and (4).

Furthermore, the simple binary nature of this synthetic system allowed its investigation by a comprehensive time-resolved ESI-MS analysis, yielding unprecedented mechanistic information regarding the initial interactions and reorganizations of the $\{\gamma\text{-SiW}_{10}\}$ precursor in the presence of Fe^{2+} .



INTRODUCTION

Polyoxometalates (POMs) represent a well explored area of inorganic metal oxide-derived materials, and they have shown potential for applications in the areas of catalysis,^{1–3} medicine,^{4,5} magnetism,^{6,7} electrochemistry,⁸ materials design^{9,10} and as models for self-assembling nanoscale systems.¹¹ The structure of molecules determines their function, and this applies to POMs also. It follows that if the structure of POMs could be rationally designed, then the engineering of POMs to a particular function becomes a real possibility. At present, however, the a priori design of POMs is still far from reach, as there is still much left to understand regarding the superficially facile assembly of POMs and the complex relationships between synthetic parameters, crystallization methods and the resulting final architectures. One particular structural and synthetic challenge in POM chemistry is the selective generation of isomeric architectures.

One class of POMs with a rich array of potential applications is transition metal substituted POMs (TMSPs). The incorporation of TMs into POM architectures facilitates the formation of elaborate and intricate structures, due to their variable coordination number and geometry, but also proffers more interesting physical properties, due to the variable electronic and magnetic states of the incorporated TMs.^{12–16} One method to obtain TMSPs is to use preformed lacunary polyoxotungstate (POT) starting materials. Such POTs have geometrically defined vacant sites to accommodate other metals; however, lacunary POTs are known to reorganize in solution, which helps to introduce structural diversity, but also

greatly increases the complexity of the reaction mixture, thus obstructing our capacity to understand it.^{17–19}

A key challenge encountered in cluster synthesis is control over both the assembly of the lacunary precursors and the coordination of POMs to transition metals on the molecular level. Typically, a great deal of effort is used to control multiple synthetic parameters at once, typically via chemical means, but this further increases the complexity of TMSP reactions and makes it more difficult to postulate and determine the likely mechanisms underlying the assembly processes. In contrast to this traditional approach, we report the synthesis of a series of Fe based TMSPs formed only by mixing $\text{K}_8[\gamma\text{-SiW}_{10}\text{O}_{36}]$ and $\text{FeCl}_2 \cdot 4\text{H}_2\text{O}$ in water. This simple reaction system allowed us to examine, in unprecedented detail, the innate reactivity between transition metals and lacunary POTs.

DISCUSSION

The addition of $\text{FeCl}_2 \cdot 4\text{H}_2\text{O}$ to an aqueous solution of $\text{K}_8[\gamma\text{-SiW}_{10}\text{O}_{36}] \cdot 12\text{H}_2\text{O}$ in differing Fe:POM ratios with only 5 min stirring time led to the isolation of four new iron-substituted POMs. At lower iron content two isomeric clusters formed, $\text{K}_{10}\text{H}[\text{Fe}^{\text{III}}(\text{H}_2\text{O})_2\{\gamma\text{-Fe}^{\text{III}}\text{SiW}_9\text{O}_{34}(\text{H}_2\text{O})\}_2] \cdot 26\text{H}_2\text{O}$ (1) and $\text{K}_8\text{H}_3[\text{Fe}^{\text{III}}(\text{H}_2\text{O})_2\{\gamma\text{-Fe}^{\text{III}}\text{SiW}_8\text{O}_{33}(\text{H}_2\text{O})_2\}\{\gamma\text{-SiW}_{10}\text{O}_{35}\}] \cdot 42\text{H}_2\text{O}$ (2) (shown in Figure 1). These clusters represent significantly transition metal enriched analogues of a known POT architecture.²⁰

Received: July 6, 2014

Published: August 13, 2014

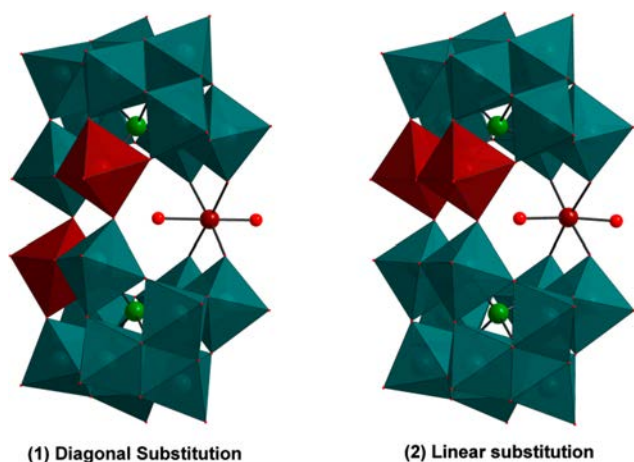


Figure 1. Polyhedral representation of isomeric anions (1) and (2). (Color scheme: W = teal, Fe = dark red, Si = green, O = red).

Cluster (1) is composed of two monosubstituted $\{\gamma\text{-SiW}_9\}$ fragments. These two Keggin fragments are connected via a $\{\text{Fe}^{\text{III}}(\text{H}_2\text{O})_2\}$ unit on one side of the cluster and by nonprotonated Fe–O–W bonds on the other, to create a diagonal substitution pattern of Fe in the cluster. Note that crystals have been identified with the diagonal substitution along either diagonal, (1a) and (1b), and each type has a different unit cell, but they are not separable from one another due to their similar size, color and general appearance. Furthermore, while each unit cell shows a definite bias for iron substitution along one diagonal, the crystals are not strictly enantiomeric. The diagonal region shows disorder in which a primary Fe diagonal shows occupancy of 90:10% Fe:W, while the counter diagonal shows 10:90% Fe:W. It is hypothesized that this disorder is due to cocrystallization of both diagonally substituted clusters within all types of crystal, though each unit cell clearly possesses a strict bias for one form.

Cluster (2) has a similar architecture to the previously reported $\{\text{Co}_4\text{Si}_2\text{W}_{18}\}$ cluster but with less transition metal present,²¹ and is composed of an intact $\{\gamma\text{-SiW}_{10}\}$ fragment and a disubstituted $\{\text{B-}\beta\text{-SiW}_8\}$ fragment. Like cluster (1), the two fragments are connected via a $\{\text{Fe}^{\text{III}}(\text{H}_2\text{O})_2\}$ unit on one side and hinged, in this case, by protonated Fe–O(H)–W bonds on the other side, which creates a linear substitution pattern of Fe. The only synthetic difference between the clusters is that cluster (1) forms when a ratio of 4:5 Fe: $\{\gamma\text{-SiW}_{10}\}$ is employed and cluster (2) when the ratio is 7:5. The isomeric clusters (1) and (2) represent the previously unrealized forms of the proposed building blocks discussed in our previous research.²²

Each $\{\text{Fe}_3\text{Si}_2\text{W}_{18}\}$ cluster comprises 18 tungsten centers and 3 iron centers. Bond valence sum (BVS) calculations revealed that all the W atoms were in the +6 oxidation state and all the Fe atoms were in the +3 oxidation state. This means that during the reaction and crystallization time the iron underwent oxidation which could be tracked visibly as the solution mixture gradually turned from brown to yellow over 1 day. Each Fe^{III} atom terminates with a water molecule (again determined by BVS calculations) and not a terminal $\text{M}=\text{O}$ as is found for the tungsten atoms.

Consistent with the findings of Bassil et al.²⁰ the Fe–O bond lengths for the sandwiched $\{\text{Fe}^{\text{III}}(\text{H}_2\text{O})_2\}$ unit are non-equivalent, with the internal water ligand being farther from the Fe^{III} atom than the external water ligand. The effect is more pronounced for compound (1) where the substitution of iron

in the cluster is diagonal ($\text{Fe}-\text{OH}_{2(\text{internal})} = 2.256 \text{ \AA}$, $\text{Fe}-\text{OH}_{2(\text{external})} = 1.989 \text{ \AA}$) compared to ($\text{Fe}-\text{OH}_{2(\text{internal})} = 2.165 \text{ \AA}$, $\text{Fe}-\text{OH}_{2(\text{external})} = 2.129 \text{ \AA}$) for the linearly substituted compound (2). For comparison, the Fe–OH₂ bond lengths for the embedded Fe^{III} atoms in the architectures are 2.018 and 2.020 \AA in compound (1) and 1.965 \AA for both Fe atoms in compound (2). The disparity in bond length is due to electronic reasons as the internal water ligand is coordinated to potassium cations on the cluster.²⁰

The degree of control over the transition metal substitution patterns in these isomeric clusters is unprecedented for TMSPs of this kind. The difference between the isomers might at a glance appear trivial, but is actually quite profound. In order to achieve the different patterns of substitution, different lacunary fragments, namely $\{\gamma\text{-SiW}_{10}\}$, $\{\gamma\text{-SiW}_9\}$ and $\{\text{B-}\beta\text{-SiW}_8\}$, must first be generated. The parent POM, $\{\gamma\text{-SiW}_{10}\}$, is known to reorganize into many different fragments,¹⁸ and several combinations of fragments are known to form together,^{19,23–25} but it is difficult to predict which fragments will form and harder still to engineer a selective control over the reorganization process in order to trap desired fragments in a final architecture. This very simple system shows that controlled crystallization of particular fragments is possible without the need for excessive manipulation of experimental parameters and further investigation of similar low parameter POM syntheses may reveal more of the subtle complexities open to lacunary POMs and their reactions with transition metals.

By increasing the amount of $\text{FeCl}_2 \cdot 4\text{H}_2\text{O}$ added to the system, dimeric species based upon (1) and (2) were able to form. A dimer of compound (2) could be formed in highest yield for a ratio of 5:2 Fe: $\{\gamma\text{-SiW}_{10}\}$. The small needle shaped crystals that form after 1–2 days can be represented by the formula $[\text{K}_{13}\text{Fe}^{\text{III}}\text{H}_{10}[\{\text{Fe}^{\text{III}}(\text{H}_2\text{O})_2(\text{SiW}_{10}\text{O}_{35})-(\text{SiFe}^{\text{III}}_2\text{W}_8\text{O}_{35})\}_2(\text{Fe}^{\text{III}}_4\text{O}_4(\text{H}_2\text{O})_6)] \cdot 35\text{H}_2\text{O}]$ (3) and the structure is shown in Figure 2.

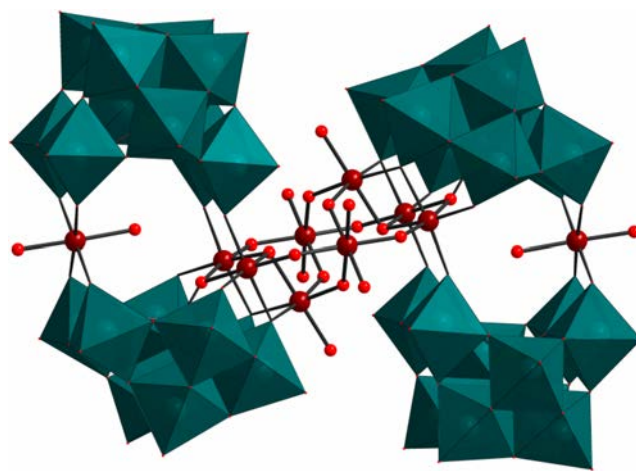


Figure 2. Representation of the dimeric cluster (3). (Color scheme: W = teal, Fe = dark red, Si = green, O = red).

While (3) is essentially a dimer of (2) bridged by four additional Fe-centers, it can be best described as a core of eight Fe^{III} atoms (confirmed by BVS) connected by eight $\mu_2\text{-OH}$ groups and two $\mu_3\text{-OH}$ groups and terminated by six water ligands. The $\{\text{Fe}_8\}$ core is encapsulated by one $\{\gamma\text{-SiW}_{10}\text{O}_{36}\}$ and one $\{\text{B-}\beta\text{-SiW}_8\text{O}_{31}\}$ unit on either side, with the $\{\text{W}_{10}\}$ and

{W₈} fragments being bridged by additional {Fe^{III}(H₂O)₂} units. These {Fe^{III}(H₂O)₂} units exhibit a similar disparity in Fe–OH₂ bond length to the monomeric species (2) (Fe–OH_{2(external)} = 2.065 Å, Fe–OH_{2(internal)} = 2.184), albeit with a more pronounced disparity for the dimeric species.

In certain instances, and optimally for a ratio of 17:10 Fe:POM, when the mother liquor that gives (3) is filtered and left to crystallize for longer, a new compound (4) forms, K₁₄[W₃₆Si₄Fe^{III}₁₀O₁₃₆(OH)₄(H₂O)₈].35H₂O. This structure is analogous to the “assembly isomers” reported in our previous research²² and can be imagined as the pairing of two clusters of (1), sandwiched by four additional Fe^{III} ions to give a Keggin-like core of composition {Fe^{III}₈W₄} (see Figure 3). The four

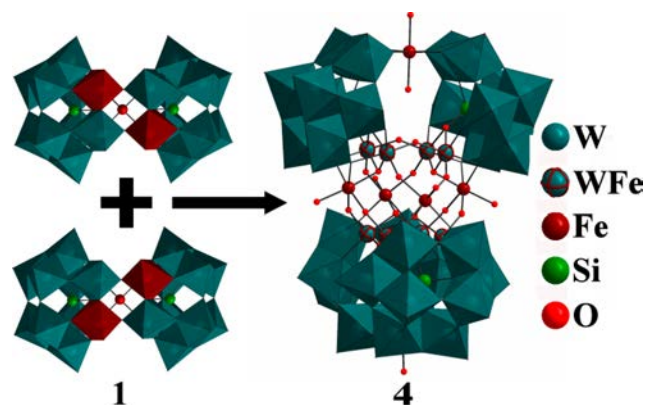


Figure 3. Representation of dimeric cluster (4). The positional disorder can be explained by the use of two differently substituted building blocks (left). (Color scheme: W = teal, Fe = dark red, W/Fe = teal ellipsoid with dark red surround, Si = green, O = red).

positions above and below the sandwiched Fe^{III} ions show a disorder of 50:50 Fe:W which would be consistent the crystal structure containing clusters comprising both diagonally substituted forms of cluster (1). BVS calculations have shown all the Fe centers to be in the 3+ oxidation state. The Fe–OH₂ distances for the {Fe^{III}(H₂O)₂} units are Fe–OH_{2(external)} = 2.071 Å and Fe–OH_{2(internal)} = 2.115 Å, which is a less pronounced disparity in bond length relative to the monomer (1).

Crystals of (3) form in 1–2 days and are very small yellow rods. Comparatively, the crystals of (4) are very large yellow rods and take 1–2 months to form, this means that the clusters can easily be separated from one another. In fact all of the clusters (1)–(4) have significantly different appearances which make them easy to identify and check for purity. Microscope images of the different crystal morphologies with indicative crystallization times are displayed in Figure 4. The effect of changing the crystallization container was investigated, by filtering the reaction mixture into either a wide-necked 50 mL conical flask, 50 mL beaker or 14 mL vial and leaving in an 18 °C temperature controlled room. It was discovered that while all the compounds crystallized in the conical flask and beaker, only compound (3) could crystallize successfully in the vials. This rudimentary experiment shows the crucial (though largely unreported) importance of crystallization methods in POM synthesis and why reporting of crystallizing conditions should be as detailed as the synthetic conditions.

The differing amounts of FeCl₂·4H₂O added to the POM solution have an effect on the pH of the reaction mixture. Higher amounts of Fe correspond to a lower pH of the reaction

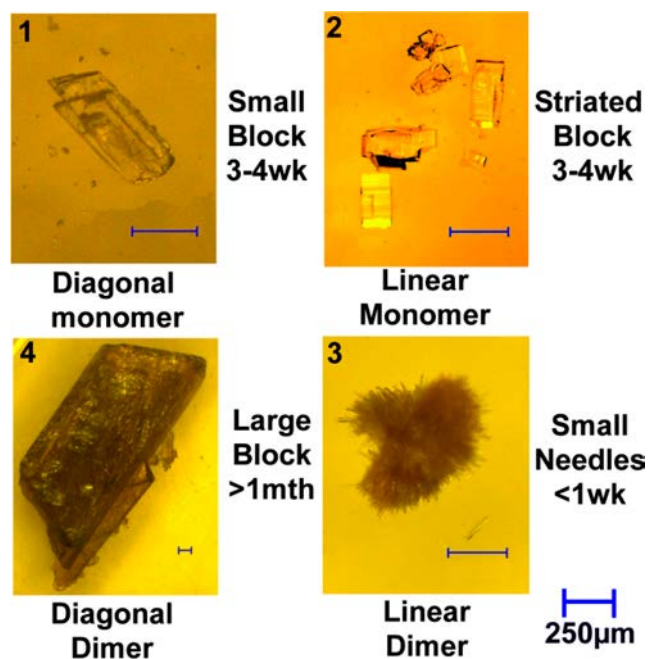


Figure 4. Photographs of the crystals clusters 1, 2, 3 and 4 taken using a digital microscope showing the difference in size and physical appearance and indicating the crystallization time.

mixture after the 5 min stirring time. This difference in pH could therefore have been one possible reason for formation of the different compounds (1–4), and so reactions were conducted in which the pH was readjusted after 5 min stirring. The reactions with low amounts of iron added were acidified with 0.1 M HCl to simulate the pH of the reactions with increased amount of iron. Conversely, the reactions with larger amounts of iron were basified by addition of 0.1 M KOH to simulate the conditions of the reactions with less iron.

Significantly, no difference in final product formation was observed for the pH adjusted reactions; however there was a noted reduction in yield. Attention was paid to the pH of the mother liquor (measured after the crystals had formed) for these pH adjusted reactions, and surprisingly, the pH value of the mother liquor was equivalent regardless of how much acid/base was added, meaning that the system must be reaching an equilibrium. The conclusion drawn from this is that it is the availability of iron ions in solution, and not the varying pH, that dictates the compounds that form and subsequently crystallize.

To analyze the solution behavior of the clusters, ESI-MS was employed on both the K⁺ salts in aqueous solution and on organic soluble tetrahexylammonium (THA) salts of the clusters, prepared via a simple ion exchange reaction using THA bromide, in MeCN solution. These organic salts gave much “cleaner” envelopes for interpretation as a result of the improved ionization of these compounds. Note that during the MS analysis it is not uncommon for fragment species to associate with sodium cations present within the spectrometer. In the case of the monomeric species (1) and (2), the major peak envelopes found at *m/z* = 1427.0 and *m/z* = 1063.3 were found to correspond to {(THA)₂K₂Na₂(Fe₃Si₂W₁₈O₆₇(OH)(H₂O)₄·10H₂O)}⁴⁻ and {(THA)K₂Na₂(Fe₃Si₂W₁₈O₆₇(OH)(H₂O)₄·8H₂O)}⁵⁻, respectively, while a well-defined series of charge-related peaks (ranging from –5 to –2) could be clearly identified in both cases. For the diagonal dimer, (4), a major peak corresponding to the intact molecular species {(THA)-

$K_5[Fe_{10}Si_4W_{36}O_{136}(OH)_4(H_2O)_8] \cdot 3H_2O\}^{7-}$ could be identified at $m/z = 1519.2$ from within a similarly well-defined series of peak envelopes ranging in charge from -7 to -3 , with m/z 4254.4 for $\{(THA)_8Na_3[Fe_{10}Si_4W_{36}O_{136}(OH)_4(H_2O)_8] \cdot 10H_2O\}^{3-}$, 3102.2 for $\{(THA)_7Na_3[Fe_{10}Si_4W_{36}O_{136}(OH)_4(H_2O)_8] \cdot 10H_2O\}^{4-}$, 2346.6 for $\{(THA)_5K_4[Fe_{10}Si_4W_{36}O_{136}(OH)_4(H_2O)_8] \cdot 7H_2O\}^{5-}$, 1896.4 for $\{(THA)_4K_4[Fe_{10}Si_4W_{36}O_{136}(OH)_4(H_2O)_8] \cdot 7H_2O\}^{6-}$ and 1574.7 for $\{(THA)_3K_4[Fe_{10}Si_4W_{36}O_{136}(OH)_4(H_2O)_8] \cdot 7H_2O\}^{7-}$ serving as the main signals. Interestingly, the linear dimer (3) was found to show a significantly different fragmentation pattern in which a minor peak at $m/z = 1594.7$ could be tentatively assigned as $\{(THA)_3KNa_5[Fe_{10}Si_4W_{36}O_{134}(OH)_{10}(H_2O)_{10}] \cdot 9H_2O\}^{7-}$; however, the breadth of the envelope and its poor resolution meant accurate absolute assignment was difficult. Furthermore, envelopes corresponding to the monomeric $\{Fe_3Si_2W_{18}\}$ -type species could be observed in the mass spectrum of (3) at $m/z = 1916.8$ for $\{(THA)_2K_3Na_3[Fe_3Si_2W_{18}O_{67}(OH)_2(H_2O)_3] \cdot 9H_2O\}^{3-}$ and 1348.5 for $\{(THA)_2K_2Na_3[Fe_3Si_2W_{18}O_{67}(OH)(H_2O)_4] \cdot 11H_2O\}^{4-}$. This therefore provides some indication of the relative stabilities of each compound and in particular the “dimeric” species (3) and (4), in which (3) seems to readily decompose into the constituent monomer species under ionization. This is unsurprising, given that the structure is much more “open” and held together by fewer bonds relative to (4), which has a compact “Keggin-like” core and is expected to provide added stability. It must also be noted that when using MS analysis, such envelopes cannot be accurately distinguished as either the diagonal or linear monomer (as they are isomeric), but given the final product (3), it is assumed they must correspond to the linear monomer (see Supporting Information section 2 for ESI-mass spectra and full peak assignments).

Given the isomeric nature of the monomers, there was a strong desire to determine the mechanism driving such a simple system to generate the different Keggin fragments and to explain the dimerization process. Such TMSP synthesis reactions are considered to be complex mixtures containing multiple Keggin fragments, some of which will be interacting with transition metals in various different coordination environments. It was therefore necessary to use a technique that would allow for an easy deconvolution of such species. Techniques such as UV and IR/Raman spectroscopy would be challenging to interpret as many Keggin species and TMSPs have similar or overlapping signals. NMR, particularly ^{183}W NMR, has the ability to differentiate all the structural species; however, the duration of a standard ^{183}W NMR analysis is considerably longer than the 5 min reaction time of this system. As it was the early stage interactions and speciations that were expected to give the most mechanistic insight, ^{183}W NMR was not considered.

The only technique that suited our purpose was mass spectrometry as it easily separates species of different charge and size and is rapid enough to measure the reactions on a suitable time scale. MS techniques have been used in the past to glean mechanistic information surrounding the formation of POMs. Most commonly the approach is to use fragmentation analysis of the final product as a means of deducing the most stable and probable building blocks and then retrofitting these results against species calculated via computational studies.^{11,26}

It was believed that studying the reaction mixture directly would give more accurate and chemically useful information from which to derive mechanistic conclusions, but doing so is difficult with traditional POM syntheses as they often involve

high ionic strength or buffered conditions, which are often incompatible with MS analysis. There is only one case where POM formation has been followed directly by MS and this was of a hybrid POM synthesized in organic medium, which is not representative of common TMSP formation.²⁷ Fortunately, the low parameter reaction system presented here was found to be ideally suited for MS analysis, as the simplicity of this scheme compared to other synthetic routes meant that there was a much lower ionic strength to the reaction. This meant that ionization and detection of POM species from the reaction mixture was relatively trivial, and, crucially given the time intensive nature of such MS analysis, the most significant reaction variable (the W:Fe ratio) could be studied in a time dependent fashion.

The reactions were conducted as normal, with 20 μ L aliquots removed at specific time intervals during the reaction and crystallization. The aliquots were diluted with 1 mL of HPLC grade water and then analyzed by ESI-MS. As a control, a solution of $K_8[\gamma-SiW_{10}O_{36}] \cdot 12H_2O$ (1.45 g, 0.5 mmol) in 30 mL of H_2O was analyzed alongside the iron reactions to corroborate which fragments were due to the starting material and which were due to the reaction with iron chloride (see Supporting Information Section 2).

The most surprising feature of the ESI-MS analysis arose from the results taken within the first hour after the addition of $FeCl_2 \cdot 4H_2O$. Previous reported hypotheses on the reorganization of $\{\gamma-SiW_{10}\}$ suggest the first step involves the loss of two W atoms to give $\{\beta-B-SiW_8\}$,²⁸ so it was anticipated that these would be the first species to present themselves as isolated species or associated with Fe ions. Rather unexpectedly, of the Keggin fragments found to have initially associated with Fe, it was the $\{FeSiW_9\}^{3-}$ (at $m/z = 869.7$: $\{K_4Na_2[FeSiW_9O_{34}(OH)_2] \cdot 5H_2O\}^{3-}$ and $m/z = 857.0$: $\{K_5Na[FeSiW_9O_{34}(OH)_2] \cdot 2H_2O\}^{3-}$) species that predominated in our analysis and over the first hour this signal diminished in intensity as the $\{Fe_2SiW_8\}^{3-}$ (at $m/z = 827.7$: $\{K_5Na[Fe_2SiW_8O_{31}(OH)_5] \cdot 4H_2O\}^{3-}$) and $\{FeSiW_{10}\}^{3-}$ (at $m/z = 910.7$: $\{K_3Na_2[FeSiW_{10}O_{36}(OH)_3(H_2O)]\}^{3-}$) signals grew (see Figure 5). A similar pattern was mirrored for the 4- signals ($m/z = 642.3$: $\{K_6[FeSiW_9O_{34}(OH)_2] \cdot H_2O\}^{4-}$ and 682.8 : $\{K_2Na_3[FeSiW_{10}O_{36}(OH)_4]\}^{4-}$) with the exception of $\{Fe_2SiW_8\}^{4-}$, which could not be identified in this region as it is either unstable at this charge or not present in large enough concentration to stand out against the “noise” of fragments in the mother liquor (see Figure S9, Supporting Information). From this observation, it is hypothesized that the reorganization of $\{\gamma-SiW_{10}\}$ to $\{B-\beta-SiW_8\}$ occurs in two steps via an intermediate $\{\gamma-SiW_9\}$ fragment. It is also worth mentioning that the directed speciation of $\{\gamma-SiW_{10}\}$ into $\{W_9\}$ and $\{W_8\}$ fragments undoubtedly occurs in response to the presence of iron ions because the time-resolved ESI-MS of the control $\{\gamma-SiW_{10}\}$ solution does not show the same detectable time-dependent correlation between these fragments. The control experiment does however show that speciation into numerous fragments appears to be instantaneous when $\{\gamma-SiW_{10}\}$ is dissolved in water (see Figure S1, Supporting Information).

Interestingly, at $m/z = 750.4$ a signal corresponding to a monosubstituted $\{K_2Na_3H_2[FeSiW_8O_{31}(OH)_3]\}^{3-}$ species could be observed. The signal is of lower intensity than the $\{Fe_2SiW_8\}$ species, but follows a similar growth pattern and is initially very weak. This has been interpreted as an intermediate species that forms from $\{\gamma-FeSiW_9\}$, via loss of W and assimilates a second iron to give the $\{\gamma-Fe_2SiW_8\}$ fragment.

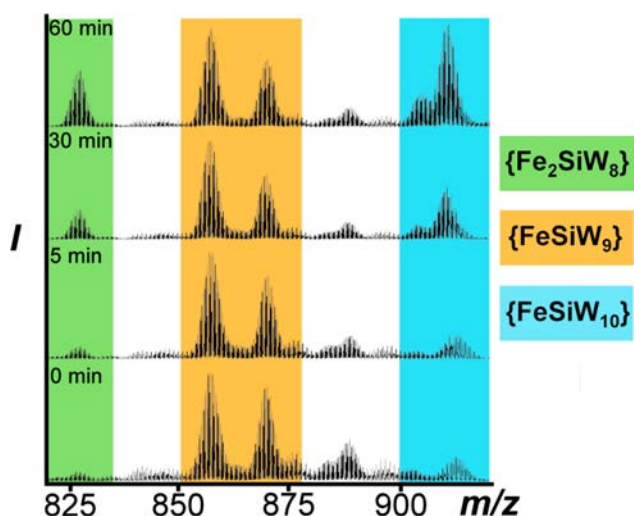


Figure 5. Change in ESI-MS of the reaction mixture/crystallization medium over 1 h. Over time the signals corresponding to $\{\text{Fe}_2\text{SiW}_8\}$ and $\{\text{FeSiW}_{10}\}$ grow in relative intensity as the originally dominant signal $\{\text{FeSiW}_9\}$ correspondingly shrinks in relative intensity. Graphs tracing the change in total ion count for these three species, for each of the four reactions are shown in the Supporting Information, Section 7.

However, it is possible that it is a fragmentation species of $\{\gamma\text{-Fe}_2\text{SiW}_8\}$ that forms due to the conditions present during the ESI-MS measurement. Combining all of the ESI-MS early stage data together, the mechanism for the formation of the required building blocks is proposed as follows. Initially $\{\gamma\text{-SiW}_{10}\}$ can either react with iron to give an $\{\text{Fe}(\gamma\text{-SiW}_{10})\}$ species, which acts as a building unit in the formation of (2), or it can undergo decomposition via loss of 1 W to give $\{\gamma\text{-SiW}_9\}$. This unit then gains 1 Fe from solution to form $\{\gamma\text{-FeSiW}_9\}$, the building block for compound (1). If this Keggin fragment loses 1 W it can form the intermediate $\{\gamma\text{-FeSiW}_8\}$ species, which gains an additional Fe to form $\{\gamma\text{-Fe}_2\text{SiW}_8\}$. The $\{\text{Fe}(\gamma\text{-SiW}_{10})\}$ and $\{\gamma\text{-Fe}_2\text{SiW}_8\}$ units can then interact to form compound (2). This process is summarized in Figure 6.

Under the standard ESI-MS conditions used in these experiments, it is also possible to observe signals representative

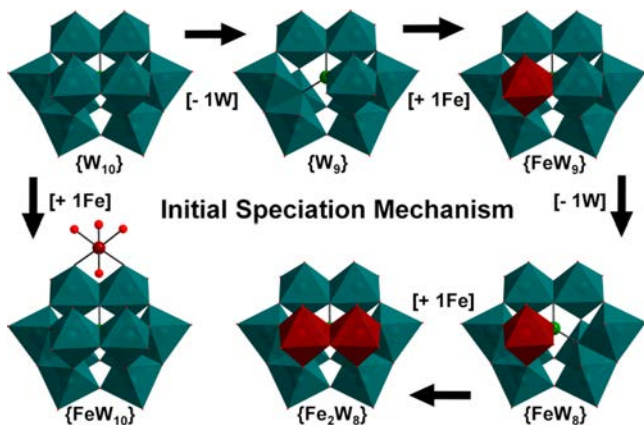


Figure 6. Polyhedral representation of the proposed mechanism for the speciation of $\{\gamma\text{-SiW}_{10}\}$ in the presence of Fe ions into the fragments required to synthesize compounds (1) and (2). The mechanism is derived from species directly observed during the ESI-MS analysis performed on the reaction mixtures. (Color scheme: W = teal, Fe = dark red, Si = green, O = red).

of the formation of the monomeric $\{\text{Fe}_3\text{Si}_2\text{W}_{18}\}$ products/building blocks but these are often poorly resolved or subsumed into the underlying background noise. However, by altering some of the key instrument parameters (i.e., by employing “softer” ionization; see Experimental Section) it was possible to observe more pronounced signals corresponding to the $\{\text{Fe}_3\text{Si}_2\text{W}_{18}\}$ units. In this way, the formation times for these products could be assessed as a function of the different amounts of iron chloride added. It was possible, therefore, to see well-defined $\{\text{Fe}_3\text{Si}_2\text{W}_{18}\}$ species after 1 h for 250 mg of FeCl_2 added. The experiments involving 140 and 170 mg FeCl_2 showed very similar spectra, with comparable $\{\text{Fe}_3\text{Si}_2\text{W}_{18}\}$ peaks occurring after 1 day. Note that for the reaction using 170 mg FeCl_2 , which can form both compounds (3) and (4), it is not possible to distinguish which isomer of $\{\text{Fe}_3\text{Si}_2\text{W}_{18}\}$ is being formed. For the reaction using 80 mg FeCl_2 it was, unfortunately, not possible to clearly observe the $\{\text{Fe}_3\text{Si}_2\text{W}_{18}\}$ units forming (analogous peaks can be identified in the same m/z region but no single isotopic envelope can be identified clearly above the underlying background), probably due to the much lower availability of iron and subsequent reduced concentration of the resulting product. The results can be summarized simply: the higher the concentration of iron in solution, the faster the $\{\text{Fe}_3\text{Si}_2\text{W}_{18}\}$ units form (a summary of the location of the $\{\text{Fe}_3\text{Si}_2\text{W}_{18}\}$ product/building block peaks can be found Figure S8, Supporting Information). As a result of the limitations of the spectrometer, under no MS conditions was it possible to observe the dimerization of (1) and (2) into (3) and (4) while monitoring the mother liquor.

Throughout these experiments, the pairings of the transient Keggin fragments into the final cluster products involves a total of three Fe cations: one sandwiched $\{\text{Fe}(\text{H}_2\text{O})_2\}$ unit and two irons embedded in the cluster architecture. None of the observed species ever showed $\{\text{Fe}_4\text{Si}_2\text{W}_{17}\}$ fragments. This would indicate that the only viable pairings are $\{\gamma\text{-FeSiW}_9\}$ with $\{\gamma\text{-FeSiW}_9\}$ (as in (1)), or $\{\gamma\text{-SiW}_{10}\}$ with $\{\gamma\text{-Fe}_2\text{SiW}_8\}$ (as in (2)). Similarly, pairing of a $\{\gamma\text{-FeSiW}_9\}$ with a $\{\gamma\text{-Fe}_2\text{SiW}_8\}$ does not appear feasible. One reason for this would be the requirement for a bridging $\mu_2\text{-O}$ to pair the clusters together. The terminal ligands on W atoms are double bonded oxo ligands, while for Fe atoms the terminal groups are water ligands. When a pairing of fragments occurs, one of the terminal ligands oxygen groups needs be eliminated and one must remain as a bridging oxo. The ideal situation would be when a W and Fe bridge. The water molecule on the iron is a labile leaving group and the $\text{W}=\text{O}$ ligand can convert into a bridging $\mu_2\text{-O}$. Fe to Fe or W to W pairings thus have less suitable ligands to facilitate bridging. This would explain why in the $\{\gamma\text{-FeSiW}_9\}$ containing clusters the iron atoms are diagonally opposite each other and not directly opposite one another. It would be expected that in a pH controlled system where protonation/deprotonation can occur, this process would be strongly influenced, and alternative pairings may be possible.

It is also important to note that the same fragments could be observed in the mass spectra for each amount of iron added, which implies that the speciation and reactivity is independent of the amount of iron added (i.e., provided there is iron in the system, these fragments will form). This begged the question as to why in each reaction did different species crystallize. It is in the aggregation of the fragments into the monomeric and dimeric species that it was hypothesized that the amount of iron present plays its largest role.

Given that over time the $\{\gamma\text{-Fe}_2\text{SiW}_8\}$ fragment predominates over the initially detected $\{\gamma\text{-FeSiW}_9\}$ species, it would appear that there is a clear preference for the formation of the disubstituted fragment. If we look at the charge density of these fragments using a simple equation employed previously by Nyman et al.²⁹ where the charge density equals the total anion charge divided by the total number of non-H atoms, then the $\{\gamma\text{-FeSiW}_9\}$ species ($[\text{Fe}^{\text{III}}(\text{H}_2\text{O})_2\text{SiW}_9\text{O}_{34}]^{7-}$) has a density of $7/47 = 0.149$, whereas the $\{\gamma\text{-Fe}_2\text{SiW}_8\}$ species ($[\text{Fe}^{\text{III}}(\text{H}_2\text{O})_2(\text{OH})\text{SiW}_8\text{O}_{31}]^{5-}$) has a density of $5/47 = 0.106$. The value for the disubstituted fragment is significantly lower and it could be this decrease of charge density that encourages the formation of the disubstituted fragment.

On a similar note, the diagonal monomer (1) ($[\text{Fe}^{\text{III}}(\text{H}_2\text{O})_2\{\gamma\text{-Fe}^{\text{III}}\text{SiW}_9\text{O}_{34}(\text{H}_2\text{O})\}\{\gamma\text{-Fe}^{\text{III}}\text{SiW}_9\text{O}_{33}(\text{OH})(\text{H}_2\text{O})\}]^{10-}$) has a density of $10/95 = 0.105$ and the linear monomer (2) ($[\text{Fe}^{\text{III}}(\text{H}_2\text{O})_2\{\gamma\text{-Fe}^{\text{III}}\text{SiW}_8\text{O}_{32}(\text{OH})(\text{H}_2\text{O})_2\}\{\gamma\text{-SiW}_{10}\text{O}_{33}(\text{OH})_2\}]^{8-}$) has a density of $8/95 = 0.084$, which are both found to be lower than the respective transient subunits and thus help to explain the monomer formation. The linear and diagonal dimer structures (3) and (4) have charge densities of 0.077 and 0.071, respectively, which continues the trend of decreasing charge density as the units aggregate into larger structures.

Given the apparent preference for the formation of $\{\gamma\text{-Fe}_2\text{SiW}_8\}$ over $\{\gamma\text{-FeSiW}_9\}$, the formation of (1) which only contains $\{\gamma\text{-FeSiW}_9\}$ fragments seems unusual. It is our current hypothesis that in the synthesis of (1), where there is less than one iron ion for every $\{\gamma\text{-SiW}_{10}\text{O}_{36}\}$ in solution, the capacity of the system to form disubstituted fragments would be reduced and compared to reactions containing more iron, there would be a significantly higher proportion of $\{\gamma\text{-FeSiW}_9\}$ fragments persisting in solution. To satisfy the desire for lower charge density, it would be more viable for these fragments to pair to give (1) directly than to form $\{\gamma\text{-Fe}_2\text{SiW}_8\}$ units as an intermediate to compounds (2) or (3). The diagonal dimer (4), which is synthesized using a higher concentration of iron chloride, only forms after the crystallization of the linear dimer (3). It is probable that following the crystallization of (3) the concentration of iron is significantly lowered which once again permits the formation diagonal monomer units, but there is most likely still more iron relative to the synthesis of (1), which would facilitate the dimerization process.

As mentioned previously, it was impossible to observe the dimerization process directly via ESI-MS analysis. Yet, from the respective crystallization times it would appear that dimerization of (2) into (3) is much quicker than the dimerization of (1) into (4). This implies that it is easier to aggregate clusters of (2) than clusters of (1). Thinking about where the incoming iron atoms would have to interact with the monomers to give the final dimeric clusters helps to explain why this should be the case. The first step in the dimerization of compound (2) would be for the monomer to gain one iron center that would interact with an $\text{Fe}-\text{O}(\text{H})-\text{Fe}$ ligand and two $\text{Fe}-\text{O}-\text{W}$ ligands to give a $\{\text{Fe}_4\text{Si}_2\text{W}_{18}\}$ structure analogous to the previously reported $[(\gamma\text{-SiW}_{10}\text{O}_{36})(\beta\text{-SiW}_8\text{O}_{30}(\text{OH}))\text{-Co}_4(\text{OH})(\text{H}_2\text{O})_7]^{10-}$ cluster.²¹ The next step would be for two additional solvated iron atoms to attach onto the cluster, each bridging one of the embedded iron atoms from (2), to the newly added Fe center. Finally, two of this unit can bond to a second $\{\text{Fe}_4\text{Si}_2\text{W}_{18}\}$ unit to complete the cluster. This process would be relatively straightforward as in each stage the cluster is

“open” and involves aggregation of iron onto iron through bridging OH ligands.

For the formation of (4) from diagonal monomer (1), the process would be conceptually more difficult. The first step could occur via one of two approaches. It could be that incoming Fe atoms interact on each $\{\gamma\text{-FeSiW}_9\}$ unit, bridging two $\text{Fe}-\text{O}-\text{W}$ ligands and one $\text{W}-\text{O}-\text{W}$ ligand in a similar fashion as described for the aggregation of (2). It is also possible that the incoming iron atoms connect across the two $\{\gamma\text{-FeSiW}_9\}$ units by bridging a $\text{W}=\text{O}$ from one subunit and an $\text{Fe}-\text{OH}_2$ ligand from the other subunit. The second option seems more likely as it involves less bond breaking and ligand loss from the incoming iron centers. Either way the final step involves two of the $\{\text{Fe}_3\text{Si}_2\text{W}_{18}\}$ species dimerizing at 90° to one another and the formation of multiple bonds between the species to give the final cluster (4). The specific orientation that the building units must have to facilitate the dimerization would make this process more difficult than the formation of (3), which may explain the significant time difference in crystallization for the dimeric clusters. The formation of (4) also requires a greater degree of ligand loss from the incoming $\{\text{Fe}(\text{H}_2\text{O})_6\}$ units than the formation of (3), but this does result in a more stable cluster (as shown via ESI-MS analysis) and lower charge density for (4). A comparison for the proposed dimerization steps involved in forming compounds (3) and (4) from (2) and (1) respectively is shown in Figure 7.

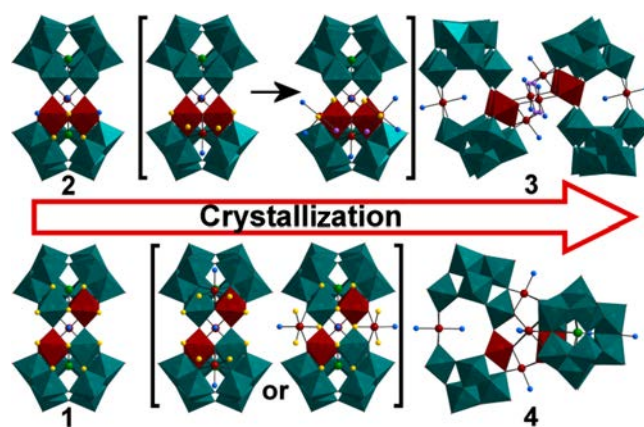


Figure 7. Polyhedral and ball-and-stick representation of the dimerization process of compound (2) into (3) and compound (1) into (4). (Color scheme: W = teal, Si = green, Fe = dark red, Water = blue, Hydroxo = purple; sites where bonding is required are shown in yellow). (*Larger image provided as Figure S12, Supporting Information).

The results presented here arise as a consequence of an unprecedented combination of time-resolved ESI-MS studies and detailed postsynthetic structural analysis that point toward a complex, equilibrium driven system in which the initial speciation products are somewhat interconvertible. There appears to be competing driving force between the favorable formation of more highly substituted fragments and the aggregation of the fragments into monomeric $\{\text{Fe}_3\text{Si}_2\text{W}_{18}\}$ and dimeric $\{\text{Fe}_{10}\text{Si}_4\text{W}_{36}\}$ TMSP species. The concentration of free iron in solution appears to be the primary structure determining factor governing this system. These simultaneously competing processes are clearly identifiable in the mass spectra of each reaction mixture, in which every possible fragment appears to be formed and present, regardless of the final

outcome, and are further manifested in the notably reduced yields of these compounds. It is believed that this system represents a strong example of the intricate complexity associated with the assembly of POM species, in which a wide range of diverse, high-nuclearity products could be synthesized from a very simple binary reaction mixture. It is remarkable that this minimal synthetic approach, in which a single variable governs the assembly of all four products, has allowed for positional control of transition metal atoms within the resulting isomeric assemblies.

Following on from the simple aqueous system, experiments were conducted using different ionic strength solutions as the reaction medium. When NaCl solutions were used, no crystalline products could be obtained. Using 0.5 and 1 M KCl solutions it was possible to isolate a mixed valence form of compound (1) regardless of how much iron chloride is added. This isomeric architecture (1') differs in that the sandwiched $\{\text{Fe}(\text{H}_2\text{O})_2\}$ unit comprises an Fe^{2+} ion, which is reduced relative to (1). The remaining Fe ions embedded in the architecture are in the +3 oxidation state, as confirmed by BVS calculations. The crystals from these reactions are dark brown and form overnight. It is hypothesized that the reason for the sole formation of this cluster is that the high ionic strength limits the solubility of the POM and iron chloride in solution and thus replicates the conditions for compound (1). The high K^+ concentration also promotes rapid crystallization which allows for the trapping of Fe^{2+} before it can oxidize fully to Fe^{3+} and the trapping of $\{\gamma\text{-FeSiW}_9\}$ clusters while they are still at high concentration.

If the reaction medium is changed to 1, 2 or 4 M LiCl then a completely new cluster forms $\text{K}_{10}\text{Li}_{12}[\text{Fe}^{\text{III}}_{0.33}\text{Cl}_2\{\beta\text{-Fe}^{\text{III}}_2\text{SiW}_{10}\text{O}_{38}(\text{OH})\}_3]\cdot 50\text{H}_2\text{O}$ (5). This cluster comprises three $\{\beta\text{-Fe}_2\text{SiW}_{10}\}$ units interconnected via $\text{Fe}-\text{O}(\text{H})-\text{Fe}$ bonds to create an internal planar hexagon of Fe^{III} atoms (see Figure 8). Other $\{\text{M}_6\text{Si}_3\text{W}_{30}\}$ clusters of POMs are known,^{30–32} but this is the first to present the β -Keggin fragment. The center of the cluster appears to be occupied by an $\{\text{FeCl}_2\}$ unit, which is confirmed by elemental analysis, but there is crystallographic disorder that makes this unit hard to assign accurately (see Figure S11, Supporting Information). Regard-

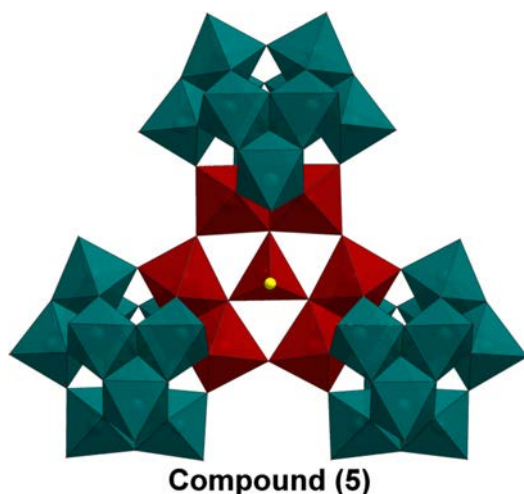


Figure 8. Polyhedral representation of Compound (5). The $\{\beta\text{-Fe}_2\text{SiW}_8\}_3$ triangular cluster contains an apparent $\{\text{FeCl}_2\}$ unit within the central cavity. (Color scheme: W = teal, Fe = dark red, Si = green, Cl = yellow).

less of the amount of FeCl_2 added to the LiCl based reactions, this cluster formed. The strong difference in architecture between (5) and the aqueous reactions (1)–(4) shows that the controlling parameters for lacunary POM reorganization and TMSP assembly change in accordance with the chemical system. Uncovering how best to control each reaction system should be paramount for ushering in a new age in POM synthesis where compound design is attainable. It was discovered that raising the pH of the reaction mixture of (5) lead to increased yields compared to the unadjusted reaction mixture, which shows that for the LiCl system, pH control is more important than in the aqueous system and perhaps the higher pH promoted the isomerization of $\{\gamma\text{-SiW}_{10}\}$ to $\{\beta\text{-SiW}_{10}\}$.

The higher ionic strength solutions add extra complexity to the reaction system, but surprisingly the consequence appears to be a reduction in the complexity of the potential products. In the KCl and LiCl reactions the amount of iron added ceased to be a controlling parameter and regardless of the amount of iron present only one product could be obtained, compared to four in the purely aqueous system, which represents stronger product selectivity. By understanding which parameters have dominant effects over the competing processes of POM speciation and product selectivity, and how best to employ such parameters, it becomes a real possibility that POM design, both architectural and functional, can be achieved.

■ EXPERIMENTAL SECTION

$\text{K}_8[\gamma\text{-SiW}_{10}\text{O}_{36}]\cdot 12\text{H}_2\text{O}$ was prepared according to the literature procedure.³³ $\text{FeCl}_2\cdot 4\text{H}_2\text{O}$ was provided by Sigma Aldrich and used without further purification.

Preparation of Compound (1). To a solution of $\text{K}_8[\gamma\text{-SiW}_{10}\text{O}_{36}]\cdot 12\text{H}_2\text{O}$ (1.45 g, 0.5 mmol) in 30 mL of deionized water, stirring in a 100 mL beaker was added $\text{FeCl}_2\cdot 4\text{H}_2\text{O}$ (0.08g, 0.4 mmol) to give a brown solution. The solution was stirred for 5 min at RT ($\sim 21^\circ\text{C}$), after which time the pH was recorded as 6.5). The brown solution was filtered into a wide-necked 50 mL conical flask and left to crystallize at 18°C in a temperature controlled room. The solution turned from brown to yellow after 24 h. Yellow block crystals were obtained after 3–4 weeks. Yield = 81 mg, 0.014 mmol (6% based on W). Elemental analysis: $\text{Fe}_3\text{H}_{61}\text{K}_{10}\text{O}_{98}\text{Si}_2\text{W}_{18}$, MW = 5553.52 g mol⁻¹. Calculated (%): Fe (3.01), K (7.04), W (59.6). Found (%): Fe (3.30), K (6.88), W (59.6). TGA (25–450 $^\circ\text{C}$): Water loss calculated (%): 8.4. Found (%): 7.8. Characteristic FT-IR (powder) bands (cm^{-1}): 3410 (b), 1608 (b), 1003 (s), 982 (w), 941 (m), 899 (m), 860 (sh), 734 (w), 687 (w), 673 (w), 611 (w).

Preparation of Compound (2). To a solution of $\text{K}_8[\gamma\text{-SiW}_{10}\text{O}_{36}]\cdot 12\text{H}_2\text{O}$ (1.45 g, 0.5 mmol) in 30 mL of deionized water, stirring in a 100 mL beaker was added $\text{FeCl}_2\cdot 4\text{H}_2\text{O}$ (0.14g, 0.7 mmol) to give a brown solution. The solution was stirred for 5 min at RT ($\sim 21^\circ\text{C}$) after which time the pH was recorded as 5.8). The brown solution was filtered into a wide-necked 50 mL conical flask and left to crystallize at 18°C in a temperature controlled room. The solution turned from brown to yellow after 24 h. Yellow plate crystals with distinct linear striations were obtained after 3–4 weeks. Yield = 248 mg, 0.043 mmol (17% based on W). Elemental analysis: $\text{Fe}_3\text{H}_{95}\text{K}_8\text{O}_{114}\text{Si}_2\text{W}_{18}$, MW = 5765.59 g mol⁻¹. Calculated (%): Fe (2.90), K (5.43), W (57.40). Found (%): Fe (3.13), K (5.15), W (56.4). TGA (25–450 $^\circ\text{C}$) conducted on partially dehydrated sample $\text{Fe}_3\text{H}_{81}\text{K}_8\text{O}_{100}\text{Si}_2\text{W}_{18}$. Water loss calculated (%): 9.7. Found (%): 9.4. Characteristic FT-IR (powder) bands (cm^{-1}): 3373 (b), 1624 (b), 1419 (b), 1001 (m), 943 (m), 864 (sh), 831 (w), 731 (w), 688 (w), 619 (w).

Preparation of Compound (3). To a solution of $\text{K}_8[\gamma\text{-SiW}_{10}\text{O}_{36}]\cdot 12\text{H}_2\text{O}$ (1.45 g, 0.5 mmol) in 30 mL of deionized water, stirring in a 100 mL beaker was added $\text{FeCl}_2\cdot 4\text{H}_2\text{O}$ (0.25g, 1.25 mmol) to give a brown solution. The solution was stirred for 5 min at RT ($\sim 21^\circ\text{C}$), after which time the pH was recorded as 5.4). The brown solution was

filtered into a wide-necked 50 mL conical flask and left to crystallize at 18 °C in a temperature controlled room. The solution turned from brown to yellow after 24 h. Thin yellow needle crystals were obtained in discrete "islands" after 2 days. Yield = 63 mg, 5.7×10^{-3} mmol (4.5% based on W). Elemental analysis: MW = 10978.4 g mol⁻¹. Calculated (%): Fe (5.60), K (4.63), W (60.3). Found (%): Fe (6.06), K (4.29), W (59.8). TGA (25–450 °C). Water loss calculated (%): 5.7. Found (%): 6.2. Characteristic FT-IR (powder) bands (cm⁻¹): 3404 (b), 1618 (b), 997 (m), 951 (sh), 862 (s), 727 (m), 626 (w), 615 (w).

Preparation of Compound (4). To a solution of K₈[γ -SiW₁₀O₃₆] \cdot 12H₂O (1.45 g, 0.5 mmol) in 30 mL of deionized water, stirring in a 100 mL beaker was added FeCl₂ \cdot 4H₂O (0.17g, 0.85 mmol) to give a brown solution. The solution was stirred for 5 min at RT (~21 °C), after which time the pH was recorded as 5.4). The brown solution was filtered into a wide-necked 50 mL conical flask and left to crystallize at 18 °C in a temperature controlled room. The solution turned from brown to yellow after 24 h. After 2 days small needle of (3) formed. Yield = 35 mg, mmol. The mother liquor from this reaction was refiltered into a clean wide-necked 50 mL conical flask and left at 18 °C for slow evaporation. After 1–2 months, large yellow rods appear of (4). Yield = 83 mg, 0.01 mmol (6.1% based on W). Elemental analysis: Fe₁₀H₉₀K₁₄O₁₈₃Si₄W₃₆, MW = 10855.01 g mol⁻¹. Calculated (%): Fe (5.14), K (5.04), W (60.97). Found (%): Fe (5.44), K (4.10), W (61.4). TGA (25–450 °C) water loss calculated (%): 7.1. Found (%): 7.2. Characteristic FT-IR (powder) bands (cm⁻¹): 3453 (b), 2363 (w), 2332 (w), 1618 (b), 1007 (m), 955 (sh), 866 (s), 721 (m), 623 (w), 613 (w).

Preparation of Compound (1'). To a suspension of K₈[γ -SiW₁₀O₃₆] \cdot 12H₂O (1.45 g, 0.5 mmol) in 30 mL of 1 M KCl, stirring in a 100 mL beaker was added FeCl₂ \cdot 4H₂O (0.08g, 0.4 mmol) to give a brown mixture. The solution was stirred for 5 min at RT (~21 °C), after which time the pH was recorded as 5.8). The brown solution was filtered into a wide-necked 50 mL conical flask and left to crystallize at 18 °C in a temperature controlled room. The solution turned from brown to yellow after 24 h. Brown needle crystals were obtained overnight. Yield = 134 mg, 0.024 mmol (9.7% based on W). Elemental analysis Fe₃H₃₄K₁₀O₉₅Si₂W₁₈, MW = 5498.46 g mol⁻¹. Calculated (%): Fe (3.05), K (7.11), W (60.1). Found (%): Fe (3.45), K (6.76), W (58.8). TGA (25–450 °C): Water loss calculated (%): 7.5; found (%): 7.7. Characteristic FT-IR (powder) bands (cm⁻¹): 3387 (b), 1618 (b), 1001 (m), 943 (sh), 895 (w), 860 (s), 733 (w), 708 (w), 667 (w).

Preparation of Compound (5). To a solution of freshly prepared K₈[γ -SiW₁₀O₃₆] \cdot 12H₂O (1.45 g, 0.5 mmol) in 25 mL of 4 M LiCl solution was added FeCl₂ \cdot 4H₂O (0.2 g, 1.0 mmol) to give a brown solution of pH < 4. The pH was adjusted to 7.9 by dropwise addition of 2 M KOH solution and sustained at 7.9 for 5 min by dropwise addition of 0.5 M KOH, as required. The solution was stirred for a further 10 min and was then centrifuged and filtered into a clean, wide-necked 50 mL conical flask and left to slowly evaporate in a temperature controlled room at 18 °C. Overnight the mother liquor turned yellow and yielded small yellow block crystals. Yield = 105 mg, 0.01 mmol (7.5% based on W). Elemental analysis: Cl₂Fe_{6.33}H₁₀₃K₁₀O₁₆₇Si₃W₃₀, MW = 9274.02 g mol⁻¹. Calculated (%): Fe (3.81), K (4.22), W (59.47). Found (%): Fe (3.89), K (4.15), W (59.2). TGA (25–450 °C) conducted on partially dehydrated sample, Cl₂Fe_{6.33}H₇₉K₁₀O₁₅₅Si₃W₃₀ water loss calculated (%): 7.6. Found (7.3). Characteristic FT-IR (powder) bands (cm⁻¹): 3335 (b), 1615 (b), 958 (s), 875 (s), 763 (sh), 681 (w), 643 (w), 618 (w).

Preparation of THA Salts of Compounds (1–4). To make the THA salts 10 mg of the TMSP compound was dissolved in 5 mL of deionized H₂O, which was diluted with 5 mL of HPLC grade acetonitrile. To this was added 150 mg of tetrahexylammonium bromide and either precipitate or oil formed. The solid/oil was left to settle overnight, and then the solution was decanted off. The solid/oil was dissolved in 5 mL of MeCN and reprecipitated by addition of 25 mL of H₂O. The solid/oil was sedimented via centrifugation, and the reprecipitation process was conducted twice more. The resultant yellow oils were washed with 3 \times 10 mL of deionized water and dried

overnight in a desiccator, and then used directly for ESI-MS by dissolving in MeCN.

ESI-MS Experimentation. All electrospray-ionization mass spectrometry (ESI-MS) measurements were performed on a Waters Synapt G2 HDMS spectrometer operating in sensitivity/resolution modes, equipped with a quadrupole and time-of-flight (Q/ToF) module for MS analysis. All samples were prepared as described in the following and injected directly at a flow rate of 5 μ L min⁻¹ using a Harvard syringe pump. All spectra were collected in negative mode and analyzed using the Waters MassLynx v4.1 software.

THA Salt Analysis. THA salts of 1–4 were prepared by dissolving in HPLC grade CH₃CN to a concentration of ca. 1×10^{-5} M and introduced to the spectrometer via direct injection. The following parameters were employed: capillary voltage, 3.0 kV; sample cone voltage, 20 V; extraction cone voltage, 4 V; source temperature, 80 °C; desolvation temperature, 180 °C; cone gas flow, 15 L h⁻¹ (N₂); desolvation gas flow, 750 L h⁻¹ (N₂).

Mother Liquor Analysis. Aliquots of each reaction were prepared by transferring 20 μ L of the reaction mixture into a vial containing 1 mL of HPLC grade H₂O and mixing thoroughly. These samples were measured within 1 h of collection; however, control experiments performed on aged samples and on neat, undiluted mother liquor showed that the primary conclusions of our experiments were neither time- nor concentration-dependent. The following standard parameters were employed for these measurements: capillary voltage, 1.8 kV; sample cone voltage, 35 V; extraction cone voltage, 4 V; source temperature, 80 °C; desolvation temperature, 150 °C; cone gas flow, 15 L h⁻¹ (N₂); desolvation gas flow, 550 L h⁻¹ (N₂). We describe this as v1 methodology.

In order to attempt to identify higher molecular weight species (such as the fully formed {Fe₃W₁₈} clusters discussed above), a second set of lower ionization parameters was occasionally employed in which the "sample cone voltage" was set to 10 V (all other parameters remained constant). This had the effect of selecting for higher mass species and "filtered" smaller, fragmentary ions from the spectra. We describe this as v2 methodology. Unfortunately, this was not generally applicable, however, as it was found to significantly lower the signal intensity and also prevent the identification of some mechanistically important peaks. Those species which could only be identified under these settings will be highlighted as such in the appropriate peak tables.

CONCLUSIONS

The minimal parameter synthetic approach undertaken in this research facilitated the answering of several fundamental questions relating to POM assembly and formation. By exploring the simplest TMSP reactions possible, we uncovered the innate, equilibrium driven response of { γ -SiW₁₀} when introduced to a transition metal, iron. Despite the simplicity of the binary reaction system itself, the products are structurally complex and could be synthesized with high purity and in isolation of one another. Compounds (1) and (2) are isomeric but, significantly, contain different Keggin fragments; (1) being comprised solely of { γ -SiW₉} fragments (one of the rarest lacunary species reported),²² and (2) comprised of { γ -SiW₁₀} and { β -SiW₈}, a combination reported only twice before.^{19,21} This gives rise to remarkable positional control over the formation of these diagonally and linearly substituted isomers, governed by no more than a single, easily manipulated synthetic variable. This feature becomes even more pronounced as these structures dimerize to give compounds (4) and (3) respectively. Compound (4) possesses a compact structure with a Keggin-like core, whereas compound (3) shows a more open, S-shaped architecture. The difference in structure is largely due to the fact that the dimerization primarily occurs through the substituted Fe atoms, and is thus entirely dependent on the topology of the monomer precursor. Additional experiments, in which the pH was varied, show

that the selectivity of the reaction is unaffected by pH and thus convincingly arises a sole consequence of the amount of iron chloride added. Subsequent ESI-MS analysis of THA salts of compounds (1)–(4) was also able to contrast the relative stabilities of these species, in which (3) was found to be the least stable and undergoes significant decomposition as a result of its more open framework.

The most beneficial feature of these reactions was the low ionic strength, which allowed the reaction and crystallization to be followed in situ by time-resolved ESI-MS, a technique which is usually incompatible with standard TMSP syntheses. The results of the MS experiments identified particular speciation products that changed in abundance over time in the presence of iron, but not in the control reaction involving $\{\gamma\text{-SiW}_{10}\}$ alone. Identification of such transient intermediates was only possible using MS analysis and represents the first ever application of ESI-MS to directly follow the formation of TMSP clusters. The equilibrium driven speciation that could be identified thus reveals details of how $\{\gamma\text{-SiW}_{10}\}$ interacts with iron to give the fragments present in all of the final compounds, and for the first time, it was possible to directly and unambiguously observe a transformation from $\{\gamma\text{-SiW}_{10}\}$ to $\{\gamma\text{-FeSiW}_9\}$ to $\{\gamma\text{-FeSiW}_8\}/\{\gamma\text{-Fe}_2\text{SiW}_8\}$. This remarkable observation both supports and significantly adds to the previous hypothesis for the rearrangement of $\{\gamma\text{-SiW}_{10}\}$ in solution.²⁸

By changing the ionic strength of the solution to 1 M KCl, the selectivity of the reaction system was lost and only one product was obtained, (1'), a mixed valence version of compound (1). By changing the system to 4 M LiCl a completely different cluster was obtained that was comprised solely of $\{\beta\text{-Fe}_2\text{SiW}_{10}\}$ units. These results confirmed that the reaction medium itself can have a significant impact on the speciation and crystallization products that form.

Perhaps if TMSP reactions are examined from a perspective of simplicity, much can be learned about the direct influence of specific synthetic parameters upon assembly and aggregation. Of particular interest would be a comparison of how the speciation and crystalline products alter when different transition metals replace iron in this exceptionally simple aqueous system.

■ ASSOCIATED CONTENT

📄 Supporting Information

Experimental details, characterization data, and crystallographic parameters (CIF). This material is available free of charge via the Internet at <http://pubs.acs.org>.

■ AUTHOR INFORMATION

Corresponding Author

lee.cronin@glasgow.uk

Notes

The authors declare no competing financial interest.

■ ACKNOWLEDGMENTS

This work was supported by the EPSRC and the University of Glasgow. We would like to thank Dr. De-Liang Long for his contribution toward the finalized crystal structures and to thank Prof. Dr. Paul Kögerler of RWTH Aachen University for assistance with elemental analysis.

■ REFERENCES

(1) Kozhevnikov, I. V. *Chem. Rev.* **1998**, *98*, 171.

- (2) Misono, M. *Chem. Commun.* **2001**, 1141.
(3) Kamata, K.; Yonehara, K.; Sumida, Y.; Yamaguchi, K.; Hikichi, S.; Mizuno, N. *Science* **2003**, *300*, 964.
(4) Hasenknopf, B. *Front. Biosci., Landmark Ed.* **2005**, *10*, 275.
(5) Yamase, T. *J. Mater. Chem.* **2005**, *15*, 4773.
(6) Zheng, S.-T.; Yang, G.-Y. *Chem. Soc. Rev.* **2012**, *41*, 7623.
(7) Kortz, U.; Müller, A.; van Slageren, J.; Schnack, J.; Dalal, N. S.; Dressel, M. *Coord. Chem. Rev.* **2009**, *253*, 2315.
(8) Sadakane, M.; Steckhan, E. *Chem. Rev.* **1998**, *98*, 219.
(9) Coronado, E.; Gómez-García, C. J. *Chem. Rev.* **1998**, *98*, 273.
(10) Long, D.-L.; Tsunashima, R.; Cronin, L. *Angew. Chem., Int. Ed.* **2010**, *49*, 1736.
(11) Vilà-Nadal, L.; Mitchell, S. G.; Long, D.-L.; Rodríguez-Fortea, A.; Lopez, X.; Poblet, J. M.; Cronin, L. *Dalton Trans.* **2012**, *41*, 2264.
(12) Bassil, B. S.; Ibrahim, M.; Al-Oweini, R.; Asano, M.; Wang, Z.; van Tol, J.; Dalal, N. S.; Choi, K.-Y.; Ngo Biboum, R.; Keita, B.; Nadjo, L.; Kortz, U. *Angew. Chem., Int. Ed.* **2011**, *50*, 5961.
(13) Bassil, B. S.; Nellutla, S.; Kortz, U.; Stowe, A. C.; van Tol, J.; Dalal, N. S.; Keita, B.; Nadjo, L. *Inorg. Chem.* **2005**, *44*, 2659.
(14) Gaunt, A. J.; May, I.; Collison, D.; Travis Holman, K.; Pope, M. T. *J. Mol. Struct.* **2003**, *656*, 101.
(15) Pradeep, C. P.; Long, D.-L.; Kögerler, P.; Cronin, L. *Chem. Commun.* **2007**, 4254.
(16) Mitchell, S. G.; Streb, C.; Miras, H. N.; Boyd, T.; Long, D.-L.; Cronin, L. *Nat. Chem.* **2010**, *2*, 308.
(17) Chen, L.; Shi, D.; Zhao, J.; Wang, Y.; Ma, P.; Wang, J.; Niu, J. *Cryst. Growth Des.* **2011**, *11*, 1913.
(18) Bassil, B. S.; Kortz, U. *Dalton Trans.* **2011**, *40*, 9649.
(19) Mitchell, S. G.; Molina, P. L.; Khanra, S.; Miras, H. N.; Prescimone, A.; Cooper, G. J. T.; Winter, R. S.; Brechin, E. K.; Long, D.-L.; Cogdell, R. J.; Cronin, L. *Angew. Chem., Int. Ed.* **2011**, *50*, 9154.
(20) Bassil, B. S.; Dickman, M. H.; Reicke, M.; Kortz, U.; Keita, B.; Nadjo, L. *Dalton Trans.* **2006**, 4253.
(21) Lisnard, L.; Mialane, P.; Dolbecq, A.; Marrot, J.; Clemente-Juan, J. M.; Coronado, E.; Keita, B.; de Oliveira, P.; Nadjo, L.; Sécheresse, F. *Chem.—Eur. J.* **2007**, *13*, 3525.
(22) Winter, R. S.; Yan, J.; Busche, C.; Mathieson, J. S.; Prescimone, A.; Brechin, E. K.; Long, D.-L.; Cronin, L. *Chem.—Eur. J.* **2013**, *19*, 2976.
(23) Mitchell, S. G.; Miras, H. N.; Long, D.-L.; Cronin, L. *Inorg. Chim. Acta* **2010**, *363*, 4240.
(24) Botar, B.; Kögerler, P. *Dalton Trans.* **2008**, 3150.
(25) Compain, J.-D.; Mialane, P.; Dolbecq, A.; Mbomekallé, I. M.; Marrot, J.; Sécheresse, F.; Rivière, E.; Rogez, G.; Wernsdorfer, W. *Angew. Chem., Int. Ed.* **2009**, *48*, 3077.
(26) Vilà-Nadal, L.; Mitchell, S. G.; Rodríguez-Fortea, A.; Miras, H. N.; Cronin, L.; Poblet, J. M. *Phys. Chem. Chem. Phys.* **2011**, *13*, 20136.
(27) Wilson, E. F.; Miras, H. N.; Rosnes, M. H.; Cronin, L. *Angew. Chem., Int. Ed.* **2011**, *50*, 3720.
(28) Nsouli, N. H.; Ismail, A. H.; Helgadottir, I. S.; Dickman, M. H.; Clemente-Juan, J. M.; Kortz, U. *Inorg. Chem.* **2009**, *48*, 5884.
(29) Nyman, M.; Burns, P. C. *Chem. Soc. Rev.* **2012**, *41*, 7354.
(30) Botar, B.; Kögerler, P.; Hill, C. L. *Inorg. Chem.* **2007**, *46*, 5398.
(31) Bassil, B. S.; Mal, S. S.; Dickman, M. H.; Kortz, U.; Oelrich, H.; Walder, L. J. *Am. Chem. Soc.* **2008**, *130*, 6696.
(32) Kikukawa, Y.; Yamaguchi, K.; Hibino, M.; Mizuno, N. *Inorg. Chem.* **2011**, *50*, 12411.
(33) Canny, J.; Tézé, A.; Thouvenot, R.; Hervé, G. *Inorg. Chem.* **1986**, *25*, 2114.